




RESEARCH ARTICLE

10.1029/2023SW003769

Validating a UK Geomagnetically Induced Current Model Using Differential Magnetometer Measurements

J. Hübert¹ , C. D. Beggan¹ , G. S. Richardson¹ , N. Gomez-Perez¹, A. Collins¹, and A. W. P. Thomson¹ 

¹British Geological Survey, Edinburgh, UK

Key Points:

- We present Differential Magnetometer Method (DMM) data from 12 sites in the UK from which we compute line geomagnetically induced currents (GICs)
- Using ground electric fields computed using magnetotelluric impedances, we match the GIC model with the observed line GICs at the DMM sites
- We validate our highly detailed model of GIC in the UK power transmission network with these DMM measurements

Supporting Information:

Supporting Information may be found in the online version of this article.

Correspondence to:

J. Hübert,
juliane.huebert@bgs.ac.uk

Citation:

Hübert, J., Beggan, C. D., Richardson, G. S., Gomez-Perez, N., Collins, A., & Thomson, A. W. P. (2024). Validating a UK geomagnetically induced current model using differential magnetometer measurements. *Space Weather*, 22, e2023SW003769. <https://doi.org/10.1029/2023SW003769>

Received 23 OCT 2023

Accepted 6 FEB 2024

Author Contributions:

Conceptualization: J. Hübert, C. D. Beggan, G. S. Richardson, A. W. P. Thomson

Data curation: J. Hübert, C. D. Beggan, A. Collins

Formal analysis: N. Gomez-Perez

Funding acquisition: A. W. P. Thomson

Methodology: J. Hübert, C. D. Beggan, G. S. Richardson

Project administration: C. D. Beggan, A. W. P. Thomson

Software: J. Hübert, G. S. Richardson

Validation: J. Hübert, C. D. Beggan, N. Gomez-Perez

Visualization: J. Hübert

© 2024 British Geological Survey.

This is an open access article under the terms of the [Creative Commons Attribution License](https://creativecommons.org/licenses/by/4.0/), which permits use, distribution and reproduction in any medium, provided the original work is properly cited.

Abstract Extreme space weather can damage ground-based infrastructure such as power lines, railways and gas pipelines through geomagnetically induced currents (GICs). Modeling GICs requires knowledge about the source magnetic field and the electrical conductivity structure of the Earth to calculate ground electric fields during enhanced geomagnetic activity. The electric field, in combination with detailed information about the power grid topology, enable the modeling of GICs in high-voltage (HV) power lines. Directly monitoring GICs in substations is possible with a Hall probe, but scarcely realized in the UK. Therefore we deployed the differential magnetometer method (DMM) to measure GICs at 12 sites in the UK power grid. The DMM includes the installation of two fluxgate magnetometers, one directly under a power line affected by GICs, and one as a remote site. The difference in recordings of the magnetic field at each instrument yields an estimate of the GICs in the respective power line segment via the Biot-Savart law. We collected data across the UK in 2018–2022, monitoring HV line segments where previous research indicated high GIC risk. We recorded magnetometer data during several smaller storms that allow detailed analysis of our GIC model. For the ground electric field computations we used recent magnetotelluric (MT) measurements recorded close to the DMM sites. Our results show that there is strong agreement in both amplitude and signal shape between measured and modeled line and substation GICs when using our HV model and the realistic electric field estimates derived from MT data.

Plain Language Summary Space weather describes the influence of increased solar activity on the Earth and its close environment that can cause geomagnetic storms. During these, strong electrical currents in the earth are generated that can flow through the grounding points of electrical substations, causing potential damage. These currents also create an additional magnetic signal in the high voltage wires of power lines that can be measured using a very sensitive digital compass called a fluxgate magnetometer. We placed a series of these sensors at several sites in the UK. At each site, one magnetometer was placed under the power lines while a second one was located a few hundred meters away. By looking at the difference in the data between the two we can isolate the direct current flowing in the power lines. We then compared the measured current strength to a computer model developed from open source data sets of the UK power grid. The model also uses a measure for the ground electric field that is based on so-called magnetotelluric measurements. We found our model and the field measurements to match very well, giving confidence that our simulations of the whole UK grid are very close to the correct values.

1. Introduction

During severe space weather, strong enhancement of the solar wind density and the interplanetary magnetic field creates the conditions for geomagnetic storms. Rapid variations of the ground magnetic field caused by magnetosphere and ionospheric current systems will induce geoelectric fields in the subsurface (Pulkkinen et al., 2017). The magnitude and extent of the geoelectric field depends on the underlying properties of the conductivity structure (Beggan, 2015). The complex temporal and spatial magnetic field variations cause differences in the geoelectric field to arise over large areas, which can potentially reach up to several tens of volts per kilometer (V/km) in some regions of the world, particularly those overlying resistive terranes (Love et al., 2018; Myllys et al., 2014).

The widespread installation of low-resistance grounded infrastructure such as the high-voltage (HV) power transmission network, gas pipelines and railways allows the geoelectric field to equalize through the earthing points of these conductors, essentially using them as “short cuts” between distant locations. The additional quasi-steady direct currents (DC) are called Geomagnetically Induced Currents (GICs). Large GICs can represent a threat to the operation of HV transformers, for example, causing overheating and even harmonic disturbances as

Writing – original draft: J. Hübert
Writing – review & editing:
C. D. Beggan

the flux hysteresis loop inside the core is pushed into a non-linear and non-optimal performance state (Albertson et al., 1981; Boteler, 2006; Mac Manus et al., 2017; Pulkkinen et al., 2012). A well-known example of the potency of GICs is the collapse of a Quebec-Hydro network in March 1989, (Bolduc, 2002; Boteler, 2019). The cost of a widespread power outage has been estimated in the regions of many billions of US dollars per day in advanced economies (e.g., Oughton et al., 2017, 2018).

In the UK, research on space weather and its impact on ground-based infrastructure has been ongoing for over two decades. This has included research into the geophysical conditions which give rise to GICs, refining the regional electrical conductivity of the subsurface and investigating extreme scenarios (Beamish et al., 2002; Beggan et al., 2013). New innovations and improvements to the modeling of GIC in the complex UK network were developed (Kelly et al., 2017). However, validation of the network model with measurements remained difficult as data from only very few transformer sites in the UK are available (Kelly et al., 2017; Thomson et al., 2005).

Direct measurements of GICs can be made using a Hall Effect probe clamped to the earth neutral in a substation. In the past these devices are typically expensive to install and maintain across a large network. However, they are becoming more common in recent years as legislative monitoring requirements come into place and hardware becomes cheaper (Hughes et al., 2022). With the notable exception of the South Island of New Zealand where over 50 GIC monitoring sites are currently installed (Marshall et al., 2012; Rodger et al., 2017), only a few other countries report large scale deployment and/or accessibility to direct GIC data (e.g., Albert et al., 2022; Blake et al., 2018; Butala et al., 2017). An alternative method to directly measure GICs in power transmission lines for shorter time windows is to disconnect the line from the rest of the network and then using a current shunt connected between the power line and a grounding station at one of the end substations Rosenqvist and Hall (2019) and Rosenqvist et al. (2022).

The scarcity of direct GIC measurements at grounding points in UK substations makes the validation of numerical network models challenging, especially when attempting to match data from only a small number of sites and time periods which themselves may not be representative of the network as a whole, or may not be correctly calibrated. However, indirect measurements of GICs are also possible. For example, the differential magnetometer method (DMM) was first applied to pipelines by Campbell (1980) and Pulkkinen et al. (2001), and adapted later for HV power lines (Marsal et al., 2021; Matandirotya et al., 2016; Viljanen & Pirjola, 1994). With the DMM, a magnetometer placed under a HV line detects the background magnetic field plus the effect of the excess quasi-DC current flow during strong geomagnetic activity. Another magnetometer at a remote site records only the natural variation. The difference between them can be used to compute the value of GICs in the line via Ampère's Law. Another indirect approach is to measure verylow frequency (VLF) emissions from a HV transformer. Clilverd et al. (2018) have shown that multiple harmonics of 50 Hz occur when GICs flow. These methods have the advantage of being relatively inexpensive, easy to install when access to a substation can be granted and require only passive measurements to be made. It requires some additional effort to extract the absolute (rather than relative) value of GIC magnitude and it can be challenging to attribute the signal to individual transformers and/or lines.

Hübert et al. (2020) provided an overview and initial assessment of the DMM in the UK. They demonstrated that the method detected line GIC which could be reconciled with modeled GIC at a single location in the east of Scotland. This success spurred the further deployment of DMM systems across Britain between 2018 and 2022. In this study we present the results from this long running field campaign to measure line GICs across the 400 kV transmission network of mainland Britain using the DMM. This has allowed us to validate the performance of the GICs predicted with the BGS UK power grid model (Kelly et al., 2017) and proves both techniques complement each other well.

In Section 2 we describe the field sites of the DMM measurements and give a brief overview of the data collected during several periods of increased geomagnetic activity in 2018–2021. In Section 3 we briefly describe the newest version of the UK HV power grid used in the GIC computations. Section 4 follows with the validation approach taken to compare modeled and measured GIC data and several examples from geomagnetic active times during the DMM field campaign. We present the comparison and a quantitative analysis of the match between GIC data and models in the line segments monitored with DMM and additionally two Scottish substations where ground GIC data were made available by the grid operator Scottish Power Ltd. We briefly describe how in the future a higher resolution electric field model derived from new MT data will further enhance our GIC model of the UK power grid.

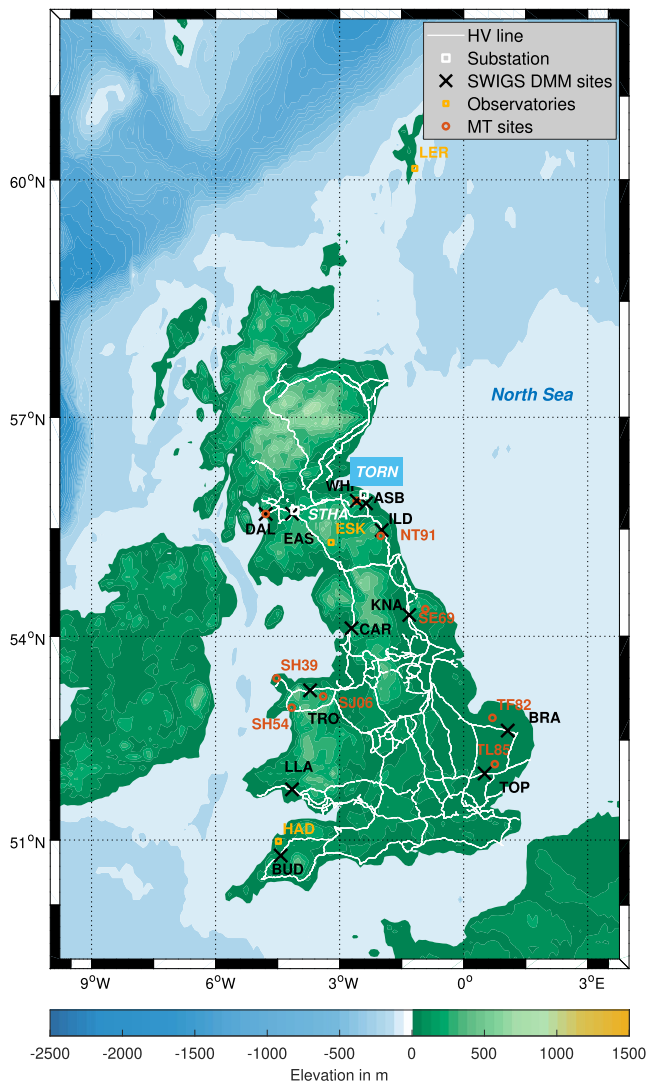


Figure 1. Elevation map of the British Isles with HV power lines, geomagnetic observatories, substations used for GIC analysis and the location of DMM and MT sites 2018–2022. Elevation data from ETOPO2 (NOAA National Centers for Environmental Information, 2022). Note that at sites *DAL* and *WHI* MT and DMM sites are in very close proximity.

2. A Differential Magnetometer Method Measurement Campaign

This study is a continuation of the work first presented in Hübert et al. (2020), where the authors presented DMM measurements and GIC modeled values for one site in Scotland for a geomagnetic storm in August 2018. Since then, we have deployed the DMM systems at 11 other sites to monitor GICs in the UK 400 kV network. The decision of where to locate each of the 11 sites was based on maximum GIC values modeled by Kelly et al. (2017), who analyzed the UK network using magnetic data from a number of historical storms. Long high-voltage power lines run along the east and west coastlines of Britain connecting power from large generation sites in the northern regions to the more populated southern areas and vice versa. The modeled GIC are highest in substations at the end of these lines. Once the HV lines with the largest GIC were identified, locations were chosen for their relative remoteness to man-made interference (e.g., urban or DC rail) to minimize electromagnetic noise from such infrastructure. Other considerations for a good site include access from a road, landowner permission, an open southerly aspect for solar panels and a consistent 3/4G mobile network connection for remote data collection.

Figure 1 shows the 400 kV line network (white lines) with the 12 DMM sites occupied over the 4 year campaign. Each site has a three letter code to describe the site (e.g., WHI is Whiteadder) and is marked by a black cross. The three UK geomagnetic observatories, Lerwick (LER), Eskdalemuir (ESK), and Hartland (HAD) are marked with open orange squares, the electrical substations Strathaven and Torness are indicated with white squares. Finally the location of nine long period magnetotelluric sites are shown as red circles. The MT sites are named after their Ordnance Survey map coordinates. Table 1 provides the name and locations of each of the DMM sites.

2.1. DMM Measurement Systems

A basic differential magnetometer method (DMM) system was described by Matandirotya et al. (2016). They placed a battery-powered magnetometer and digitizer under a single 66 kV line running across a desert in Namibia to the Obib mine. A remote magnetometer was located around 200 m from the power line. The systems ran for 6 days and during the period GIC of up to 2 A was measured.

Hübert et al. (2020) adopted a similar principle and developed six bespoke magnetometer systems. Each system consisted of a three-axis fluxgate magnetometer with a Linux-based digitizer/logger, a 4G modem, a solar panel and two deep cycle 110 Ah batteries (see Figure 1 in Hübert et al. (2020)). The magnetometers were housed in waterproof barrels buried around 1 m deep in the ground at a distance of 8 m from the power and logging electronics. Through a regulator, the solar panel charged the batteries which powered the systems overnight when no daylight was available. The 4G modem transmitted data across the mobile network to be recorded on a BGS server every 5 min.

When deployed, one magnetometer was placed directly under the HV line and the second at a sufficiently remote distance (sufficiently distanced to not pick up the GIC signal in the remote site). Underline to remote site distances varied from 80 to 300 m depending on land access and layout. From the difference of the magnetic field measured between the remote and underline magnetometers, using Biot-Savart law, it is possible to derive the direct line currents running in the cables of the HV line. For a full description of the method see Hübert et al. (2020). In the UK, most 400 kV lines carry two parallel (double) three-phase circuits. This gives six separate wires hanging from an A-frame pylon. If the lines are directly connected from one substation to another we can assume that the two circuits are balanced and that the current carried is equal.

Table 1
List of 12 DMM Site Locations and Deployment Periods

Code	Name	County	Latitude	Longitude	Deployed
ASB	Abbey St. Bathans	East Lothian	55.848°	2.360	August 2018–May 2019
BRA	Brandon Parva	Norfolk	52.637°	1.065°	February–October-2019
BUD	Bude	Cornwall	50.763°	4.425°	February–October-2020
CAR	Carnforth	Lancashire	54.113°	−2.723°	February–September-2020
DAL	Dalry	Ayrshire	55.705°	−4.791°	May 2019–June 2021
EAS	East Kilbride	South Lanarkshire	55.706°	−4.149°	May 2019–June 2021
ILD	Ilderton	Northumberland	55.482°	−1.982°	October–December-2018
LLA	Llannon	South Wales	51.765°	−4.151°	August 2021–February 2022
KNA	Knayton	North Yorkshire	54.302°	−1.314°	October-2018–September-2019
TOP	Toppesfield	Essex	52.002°	0.506°	February 2019–January 2020
TRO	Trofarth	North Wales	53.224°	−3.705°	August 2021–February 2022
WHI	Whiteadder Moor	East Lothian	55.882°	−2.586°	August 2018–April 2019

However, this is not always the case, as Hübert et al. (2020) describe. As we can only make a single integrated measurement of the magnetic field underline, it is not directly possible to separate different GIC flow from the DMM data alone if there are unbalanced current flow. In the example of Whiteadder Moor site (WHI) chosen for the first DMM deployment, the southern circuit of the double phase has a length of over 110 km while the northern circuit was much shorter at around 15 km between earthing points. It was still possible to model the expected GIC and its magnetic signature from network representation and check it against the measurements.

In general, most double circuits are balanced and the remainder of the sites at which DMM systems were deployed in Britain carried equal current which made measuring and modeling the GIC less complex.

2.2. Description of the DMM Data Set

Here we describe the data collected at our DMM sites, as captured in chronological order of installation. Geomagnetic activity is characterized by the K -index at Eskdalemuir Geomagnetic Observatory in the Scottish Borders (55.314°N, −3.206°E). Geomagnetic storm times are described using the NOAA storm G-scales. Figure 2 shows a summary of the computed GICs (as total current flowing in the three phases of each circuit) from 10 DMM sites where a significant amount of good quality data was collected. Two sites (LLA and CAR) are not shown as the data quality was poor due to equipment issues. The upper two panels show the K -index for Eskdalemuir Geomagnetic Observatory (K_{ESK} and the planetary ap index). The other panels show the daily maximum modeled GIC in the HV line as derived at each DMM site during its deployment.

The following 12 sites under 400 kV lines were surveyed:

- *Whiteadder Moor (WHI)* was installed in August 2018 on a remote moorland location in East Scotland and removed in April 2019. The double circuit runs east-west connecting a nuclear power station (Torness, TORN) and a series of large wind farms. We captured two very active periods where geomagnetic activity, characterized by the K -index at Eskdalemuir, reached values of 6. Line GICs were computed between 10 and 20 A. Data quality at both remote and underline magnetometers was excellent. A long-period MT system was installed nearby for 6 weeks in March–April 2019. As originally detailed in Hübert et al. (2020), the parallel lines at this site are not balanced, that is, only the northern line circuit is grounded at two substations close to the DMM site.
- *Abbey St Bathans (ASB)* was installed in late August 2018 and removed in May 2019 from a sheep pasture in East Scotland. Though close to WHI, the site is on a different (balanced) 400 kV line running north-south. A single wind turbine close to the site caused regular spikes in the data of both magnetometers which can be identified and removed. Two periods of $K_{ESK} > 6$ were captured during the installation time plus seven periods of lower geomagnetic activity with $K_{ESK} > 5$.

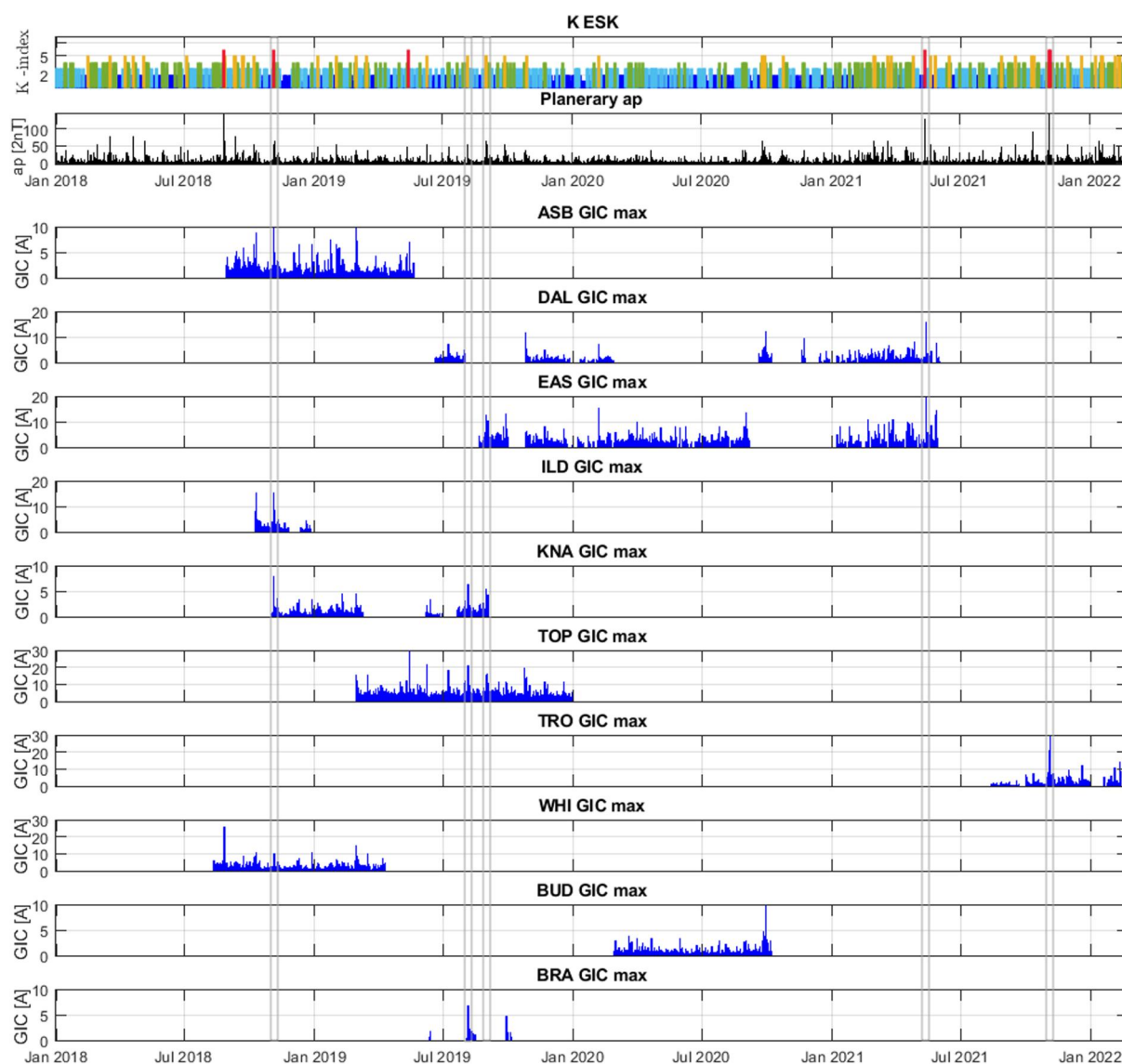


Figure 2. Geomagnetic K index at Eskdalemuir observatory and planetary ap index (in units of 2 nT) with daily GIC maximum value for each of the DMM sites 2018–2022. Periods of geomagnetic activity discussed in this paper are highlighted by the vertical gray bars.

- *Ilderton (ILD)* was installed in October 2018 on open pasture land in Northumberland. Unfortunately, the equipment was repeatedly damaged by cattle so was removed after 3 months. DMM data were collected between October and December 2018. One period of $K_{ESK} > 6$ was recorded. Maximum line GICs were 15 A.
- *Knayton (KNA)* in Yorkshire was installed on farmland in late October 2018 and removed in September 2019. A data gap from March to June 2019 was caused by livestock damage to the cabling. Data recording captured one period of geomagnetic activity with $K_{ESK} > 6$ and several periods with $K_{ESK} > 5$. Line GIC values were relatively small compared to other sites and reached 8 A during the highest geomagnetic activity.
- *Toppesfield (TOP)* in Essex was installed in late February 2019 on open farmland and recorded continuously until January 2020. It captured six periods with $K_{ESK} > 5$ and one period with $K_{ESK} > 6$. Line GICs measured were the largest observed in the field campaign with maximum values around 35 A. Data quality was good, but there we also observed strong and consistent noise signals possibly related to maintenance operation on the line as it connects to the power station in Sizewell.
- *Brandon Parva (BRA)* in Norfolk was installed in February 2019. The underline digitizer became faulty after a few days and was replaced in August 2019. Unfortunately early in October 2019 the equipment was subject to

- vandalism and theft despite being on private land in a secluded area. Therefore data collection was very limited and only one period of minor geomagnetic activity ($K_{ESK} = 5$) with line GICs around 5 A was recorded.
- *Dalry (DAL)* was installed in May 2019 in Ayrshire, Scotland on a hillside close to a recent tree plantation. In 2020, water ingress into the sensor enclosure caused damage, creating gaps in the record. After repair, the station recorded good quality data for several minor geomagnetic events. The maximum observed line GIC was 16 A on 12 May 2021 (during $K_{ESK} = 6$). A long-period MT system was installed nearby June–August 2019 to constrain the geoelectric field response at the site. The systems were removed in June 2021.
 - *East Kilbride (EAS)* was installed in May 2019 in South Lanarkshire, Scotland on flat unused land off a rural road. Substation Strathaven (STHA) is 6 km to the NE of the site. As one of the longest running DMM sites this system recorded several minor geomagnetic events with data of good quality. The maximum observed line GIC was 26 A on 12 May 2021 (during $K_p = 6$). The site was removed in June 2021.
 - *Carnforth (CAR)* in Lancashire was installed in February 2020 in a low-lying field that unfortunately flooded during unusually intense rainfall in April. Due to travel restrictions during the Covid-19 pandemic it was not possible to carry out repairs. The site was removed in September 2020.
 - *Bude (BUD)* in Cornwall was also installed in February 2020 and data were recorded until October 2020. However, 2020 was a particularly quiet period for geomagnetic activity and only one period with $K_{ESK} > 5$ was recorded. The maximum line GIC measured was 10 A.
 - *Trofath (TRO)* in North Wales was installed in August 2021 and removed in February 2022. Several minor and one severe (G4) geomagnetic storm were captured here. The maximum recorded line GIC was 30 A (during $K_{ESK} = 6$).
 - *Llannon (LLA)* in South Wales was also installed in August 2021. A faulty digitizer at the underline system prevented data collection. The remote site did record until removal in February 2022, but data were relatively noisy due to close proximity to a construction site and are not useful.

3. GIC Modeling in the UK HV Power Grid

The BGS model of the mainland Britain HV transmission network has been continuously improved and refined since 2003. Based on the pioneering work by McKay (2003) and Turnbull (2010), the initial model had 252 nodes representing substation buses or earthing points, but has now evolved to over 1,500 nodes in 2019. Transformers are represented as special connections in the model and their electrical properties are determined from the publicly available UK National Grid Electricity Ten Year Statement (ETYS, <https://www.nationalgrideso.com/research-and-publications/electricity-ten-year-statement-etys>). The 2019 ETYS had information on 1,307 transformers and details on the line connections and transformer resistances. Line resistances are computed from the transmission line impedances expressed as percentage of 100 MVA baseline in the “per-unit” representation (Saadat, 2010). The ETYS does not contain all the necessary details for creating a network, for example, there are no locations given for substations nor are the grounding resistances provided. The substation locations and line paths were discovered from online maps and satellite imagery. The grounding resistances are uniformly set to 0.5 Ω (Kelly et al., 2017).

4. Validation of GICs Based on the HV Model With DMM Data

Using the updated HV network model, line GICs and transformer earth GICs were modeled using the methodology described in Hübert et al. (2020) and Kelly et al. (2017). At each DMM site, the network model extracted from the ETYS of the year the measurements was used, that is, the 2017 model for sites ASB, BRA, ILD, TOP, WHI, KNA, the 2019 model for site EAS, the 2020 model for BUD, DAL and the 2021 for TRO. We performed analysis to determine the changes for line currents in each year's iteration of the HV model and found them to be very small (<0.5 A for a 1 V/km electric field). From the DMM measurements, we compare the modeled and measured line GICs for a number of geomagnetic events. We show five examples from periods of geomagnetic activity during 2018–2021 using data from 9 out of the 12 DMM sites.

We note that due to Covid-19 travel restrictions in much of 2020 and early 2021, it was not possible to undertake field work for several months. Repairs and maintenance at several sites could not be carried out and therefore DMM recordings at CAR and BUD cover relatively short time periods without major geomagnetic activity. The line GICs derived at these two sites were therefore quite limited and are not shown. However, we did have access to ground GIC measured at Strathaven and Torness substations using data recorded by Scottish Power Ltd. GIC

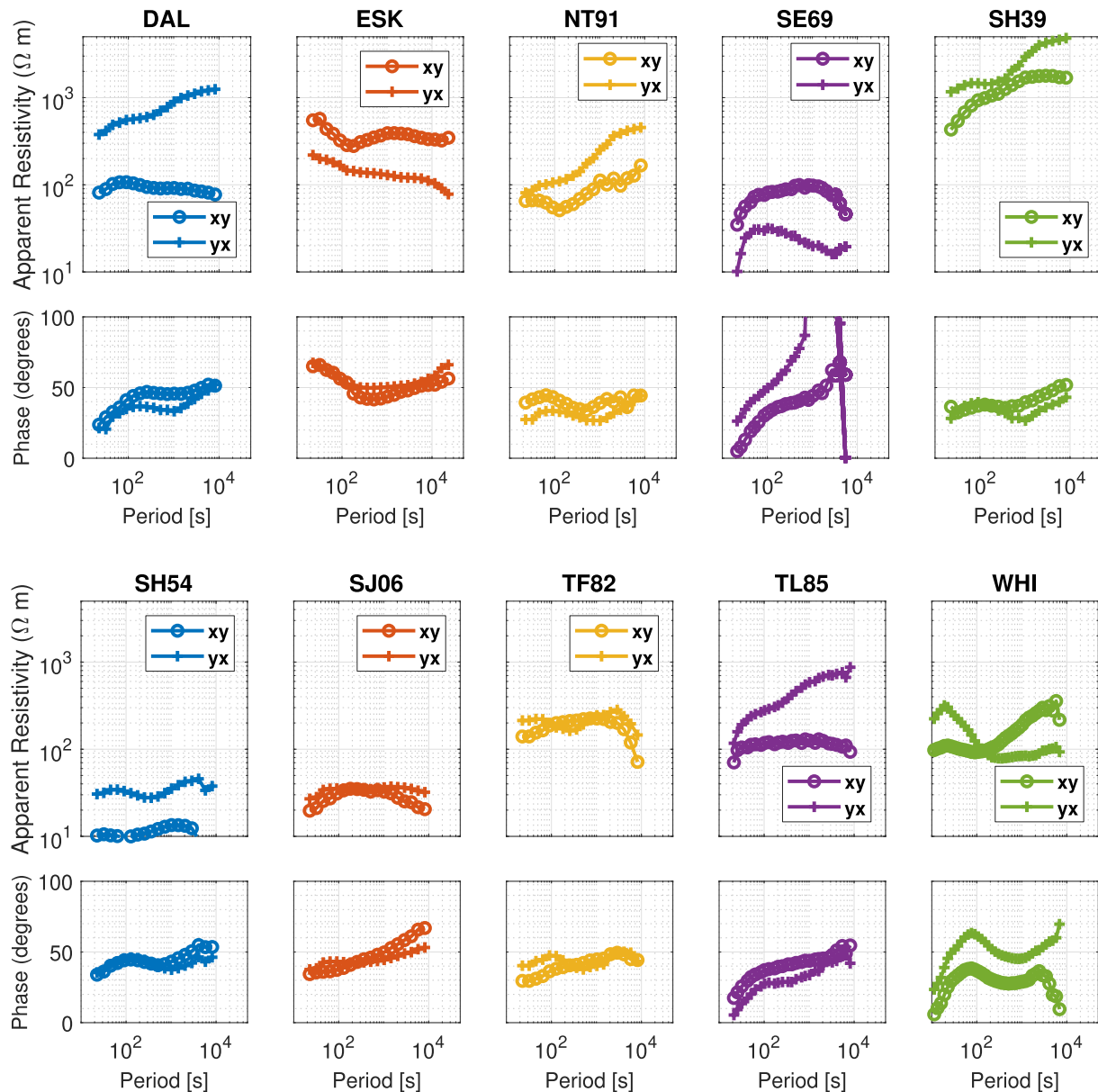


Figure 3. Apparent resistivity (upper) and phase (lower panels) of the main components Z_{xy} and Z_{yx} of the MT impedance tensor at 10 locations in the UK. The different levels of apparent resistivity curves illustrate the varying amplitude of the local geoelectric field which is controlled by regional geology. The phase values are an indicator for the complexity of the underlying conductivity distribution. For example, SE69 shows strong 3D influences in the Z_{yx} phase which changes quadrant for the longer periods.

data for several storm periods were kindly provided upon request and are used for the validation of transformer earthing point GIC computations in our model.

We also make use of magnetotelluric data collected at locations near the DMM sites to predict the local electric field during selected geomagnetic storm times. During an MT measurement, simultaneous recordings of the variations in the horizontal components of the magnetic and electric fields at each location are used to derive a transfer function between magnetic and electric fields—the complex and frequency dependent impedance tensor. Using MT impedances to model ground electric fields during geomagnetic storm times has been successfully applied in other regions of the world (Alves Ribeiro et al., 2021; Campaña et al., 2019; Love et al., 2018).

Figure 3 shows the main MT impedance, represented as apparent resistivity and phases at 10 sites across the UK (locations are shown in Figure 1). In general, higher apparent resistivity results in larger induced geoelectric field

Table 2
Correlation Coefficients R and Fit Factors $p1$ and $p2$ From the Polynomial Curve Fitting for GIC Models of the Five Periods of Geomagnetic Activity Analysed at DMM Sites and Substations

Storm	Strength	Site	R	$p1$	$p2$
5 November 2018	G2	ASB	0.7167	0.9699	0.0111
		ILD	0.84708	0.5011	0.0037
		KNA	0.92172	0.791	-0.004
		WHI	0.87525	1.1493	-0.0016
5 August 2019	G1	STHA	0.82525	0.4816	0.1274
		TORN (WHI)	0.60988	1.778	-1.875
		TORN (ESK)	0.86693	1.3407	-1.417
		KNA	0.80254	0.5578	0.005
		BRA	0.65571	0.2256	0.005
		TOP	0.92632	0.6407	0.0145
31 August 2019	G2	EAS	0.95017	0.894	0.008
		KNA	0.86107	0.5585	-0.0035
		TOP	0.89753	0.6016	0.067
		STHA	0.8158	0.4024	0.0698
12 May 2021	G3	DAL	0.96997	0.8644	-0.0038
		EAS	0.97984	0.9595	0.002
3 November 2021	G4	TRO	0.96219	0.8739	-0.0168
		STHA	0.66452	1.0386	-0.3063

in the region while more conductive areas have a lower magnitude. Comparing all sites it is evident that there is widespread variation across Britain. Dalry (DAL) in western Scotland has the largest apparent resistivity values and would therefore likely experience the highest geoelectric fields. The phase of the MT impedance relates to the rotation of the geoelectric field in relation to the magnetic field and is influenced by the complexity of the local geology in three dimensional space.

To compute the line GICs during the geomagnetic event, we used an estimate of the horizontal components of the electric field (E_x is the north-south component, E_y the east-west component) based on the convolution of the MT impedance tensor with the magnetic field data from the remote site of the DMM systems which is not influenced by the line currents running in the double circuits. Furthermore, we need an estimate for the line currents at each DMM site, I_x and I_y . These are derived from the GIC model for the UK HV grid using a uniform horizontal 1 V/km electric field (in both directions E_x and E_y). Then we can derive GICs by scaling the currents by the geoelectric field estimates for each time step (every 1 min).

$$GIC_{line}(t) = E_x(t) * I_x + E_y(t) * I_y \quad (1)$$

The local geoelectric field was derived using MT impedances from a nearby location (see Figure 1). This point estimate assuming that the electric field is constant along the entire HV line segment is a first step towards a full geoelectric field model across the whole modeling space (i.e., the island of Britain). This will be feasible after the completion of further field campaigns to collect MT data across Britain. In examples presented in this study we find it mostly sufficiently accurate to use the geoelectric field data computed from an MT site close (within 50 km) to the DMM site as representative of the line segment modeled. A modification had to be made for TRO, where the geometric interpolation of electric fields computed at three surrounding MT sites was used as the geology in this region varies strongly over a short distance (Schofield et al., 2021). As soon as a greater number of MT data covering the

whole of Britain are available, a more detailed analysis of the lateral electric field variations will be possible (Yang et al., 2021).

To assess how well our model reproduces GIC values, we estimated a polynomial curve fit between measurement and model ($f(x) = p1 * x + p2$, $f(x)$ = modeled GIC value, x = measured GIC) and the correlation factor R for each site and chosen geomagnetic storm time. The slope of the fitted curve (the $p1$ value) gives an indication for how well the amplitude of the modeled signal is recovered—when the $p1$ value is close to 1 the amplitude of the signal for the model GIC is closely matched. For $p1$ values smaller than 1 the amplitude is underestimated, for values larger than 1 it is overestimated. A large offset ($p2$) is an indicator for a worse linear fit as during filtering any offset from the individual measurements should have been removed. All results are summarized in Table 2 and discussed below. Additionally, we performed a spectral analysis to compare the measured and modeled GIC values to characterize the model fit in which frequency band. We followed Divett et al. (2020) and Rosenqvist et al. (2022), using the magnitude-squared coherence; all results can be found in Supporting Information S1.

The following sections present the data and modeling results for five different periods of increased geomagnetic activity 2018–2021. We describe how the electric field for the modeled GICs were derived and how well the model matches the data.

4.1. 4 November 2018 Storm: WHI, ASB, KNA, ILD

This event was classified as a G2 storm with a maximum K_{ESK} index of 6 ($a_p = 67$). Four of our DMM sites were recording in the north of England (ILD and KNA) and Scotland (WHI and ASB). Maximum line GICs observed on 4 November 21:22 UTM at the DMM sites were around 11 A. Electric fields were estimated from the magnetic

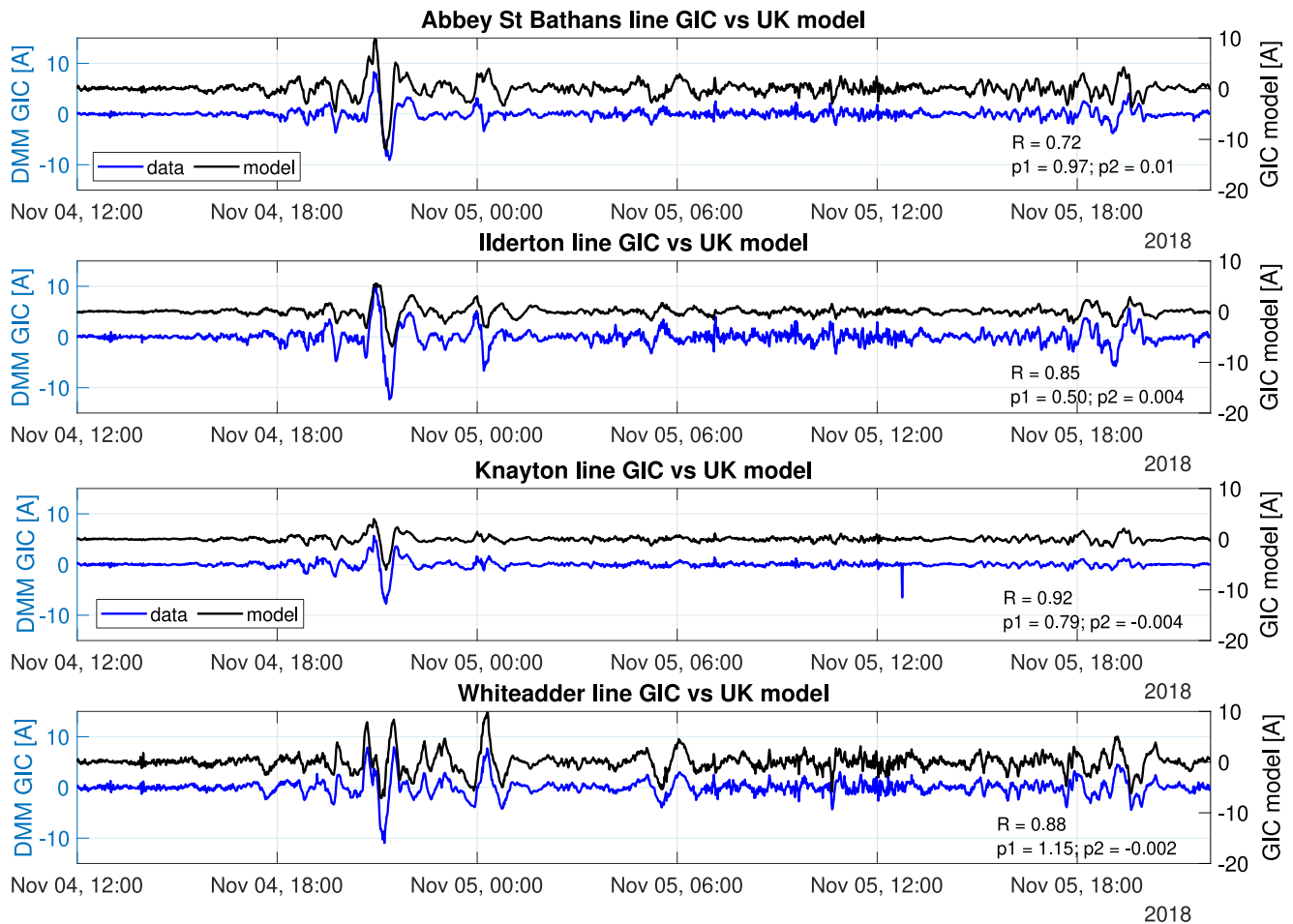


Figure 4. Measured (left axis, blue) and modeled (right axis, black) line GIC for sites Abbey St Bathans (ASB), Ilderton (ILD), Knayton (KNA), and Whiteadder (WHI) 4–6 November 2018. For better visibility, the zero line for data and model are offset. For locations see Figure 1 and Table 1. Correlation coefficient and polynomial fit coefficients are also displayed.

field variations recorded at the remote systems of the DMM sites and the MT impedance estimates derived from nearby locations (WHI, ESK, and SE69).

We compare the measured and modeled line GIC data in Figure 4. All sites show good correspondence and a high degree of correlation ranging from 0.71 to 0.92 between model and DMM estimates. The amplitude of the modeled GIC is closely matched at ASB ($p1 = 0.97$) and WHI ($p1 = 1.15$), slightly underestimated at Knayton ($p1 = 0.79$) and underestimated at Ilderton ($p1 = 0.50$).

4.2. 5 August 2019 Storm: KNA, TOP, BRA, STHA, TORN

This event was classified as a G1 minor geomagnetic storm. In the UK, local observatory data reached maximum K_{ESK} values of 5, the a_p reached 56. Three of our DMM sites were recording (KNA in North England and BRA and TOP in East Anglia). Scottish Power provided ground GIC data measured at transformers at STHA and Torness (TORN) substations in Scotland with maximum values of just below 2 A. The largest observed line GICs were very variable and ranged from 14.3 A at TOP, 5.6 A at BRA and 3.7 A at KNA on 5 August 2018 08:00 GMT.

The geoelectric fields were estimated from the magnetic field variations recorded at the remote systems of the DMM sites and the MT impedance estimates derived from nearby locations (SE69, TL85, TF82, DAL, and WHI/ESK). Comparing the measured and modeled line GIC data in Figure 5, we again see good correspondence and a high degree of correlation (R factors ranging from 0.65 to 0.92). Amplitudes are

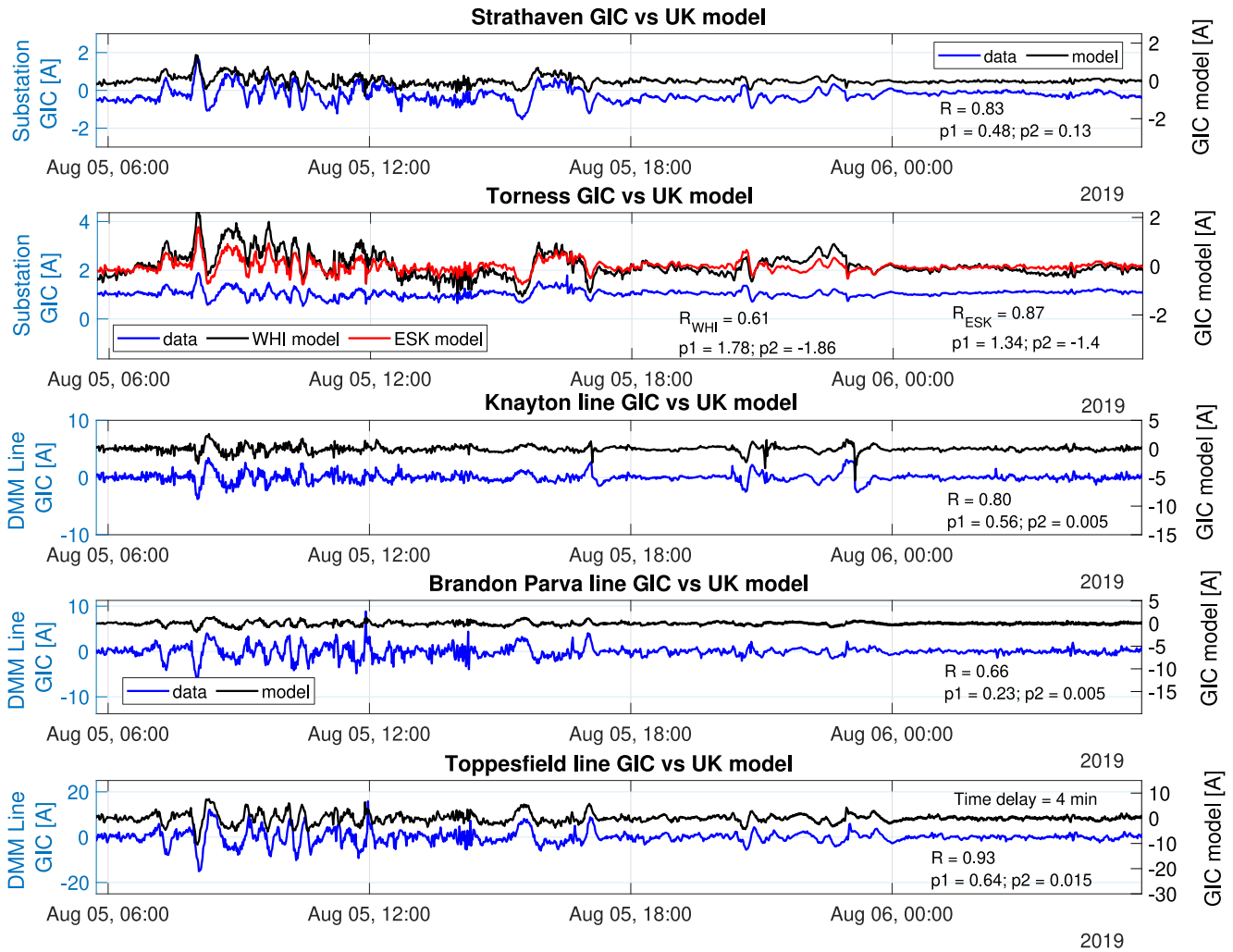


Figure 5. Measured (left axis, blue) and modeled (right axis, black) substation GIC for sites Strathaven and Torness and line GICs derived from DMM data at Knayton (KNA), Brandon Parva (BRA) and Toppesfield (TOP) 5–6 August 2019. For better visibility, the zero line for data and model are offset. For locations see Figure 1. Correlation coefficient and polynomial fit coefficients are also displayed. Substation GIC data were provided by Scottish Power Ltd.

overestimated for the ground GIC at Torness, but underestimated at Strathaven and the DMM sites. The lowest correlation value of 0.65 and underestimation of the amplitude ($p_1 = 0.23$) is likely caused by relatively poor data quality at BRA. At Torness counter-intuitively, the transformer modeled GIC data show better correlation when we use ESK (70 km away) geoelectric fields instead of WHI (30 km away) electric fields. This suggests that electric fields can be very variable even over moderate distances and can be complicated by the influence of a 3D coastline. As Torness is at the conjunction of several very long lines (>50 km) running east-west and north-south, the ESK MT impedance tensor may better represent the wider regional geoelectric field on average.

4.3. 31 August 2019 Storm: EAS, KNA, TOP, STHA

This event was classified as a G2 moderate geomagnetic storm with ESK observatory data recording maximum K values of 5, and a planetary $a_p = 67$. Three of the DMM sites were recording: EAS in Scotland, KNA in North England and TOP in East Anglia. Scottish Power provided ground GIC data measured at the substation STHA in Scotland with maximum values of below 2 A. The observed line GICs were very varied and ranged from 11.4 A at TOP, 8 A at EAS and 3.2 A at KNA on 31 August 2018 13:00 GMT.

The geoelectric fields were estimated from the magnetic field variations recorded at the remote systems of the DMM sites and with the MT impedance estimates derived from nearby locations (SE69, TL85 and DAL Figure 6)

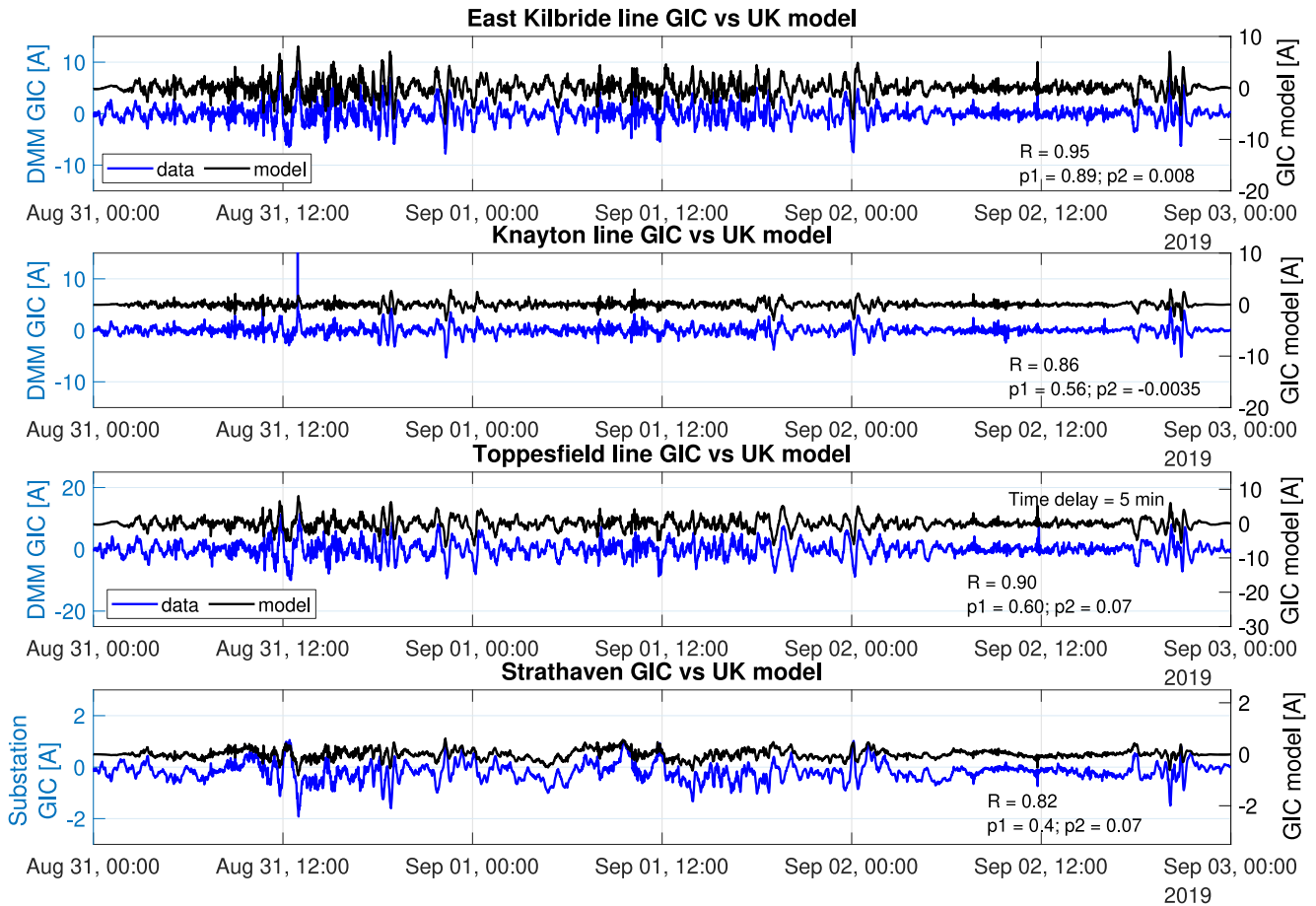


Figure 6. Measured (left axis, blue) and modeled (right axis, black) substation GIC for site Strathaven and line GICs derived from DMM data at East Kilbride (EAS), Knayton (KNA), and Toppesfield (TOP) 31 August–2 September 2019. For better visibility, the zero line for data and model are offset. For locations see Figure 1. Correlation coefficient and polynomial fit coefficients are also displayed. Substation GIC data were provided by Scottish Power Ltd.

shows very good correspondence between the modeled and measured line GICs and a high degree of correlation from 0.81 to 0.95. One slight curiosity we noted was that there is a 5 min time delay between recorded and modeled line GIC data at TOP. the modeled GIC data did also align with the other DMM sites. This was only observed for this event and is not related (as far as could be controlled) by instrument bias. This may potentially

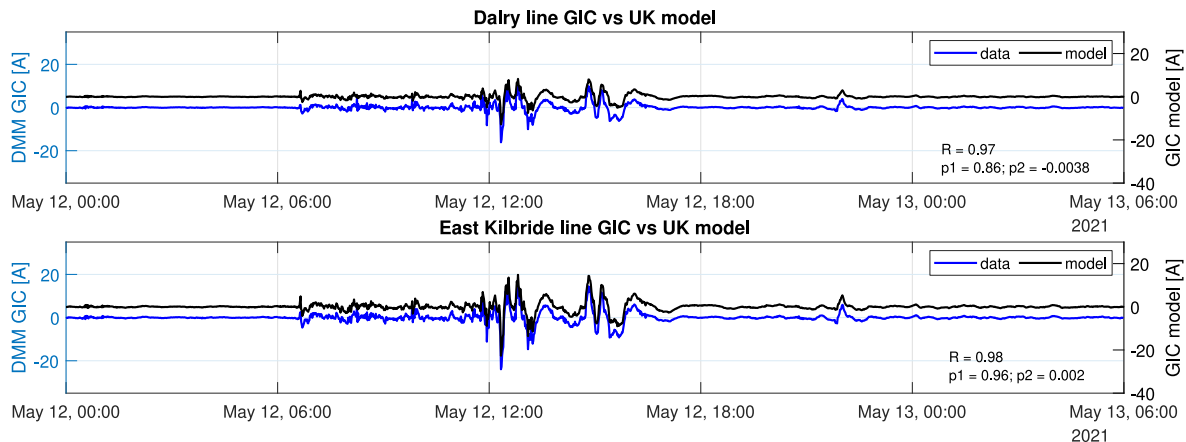


Figure 7. Measured (left axis, blue) and modeled line GICs (right axis, black) derived from DMM data at East Kilbride (EAS) and Dalry (DAL) in Scotland 11–12 May 2021. For locations see Figure 1. Correlation coefficient and polynomial fit coefficients are also displayed.

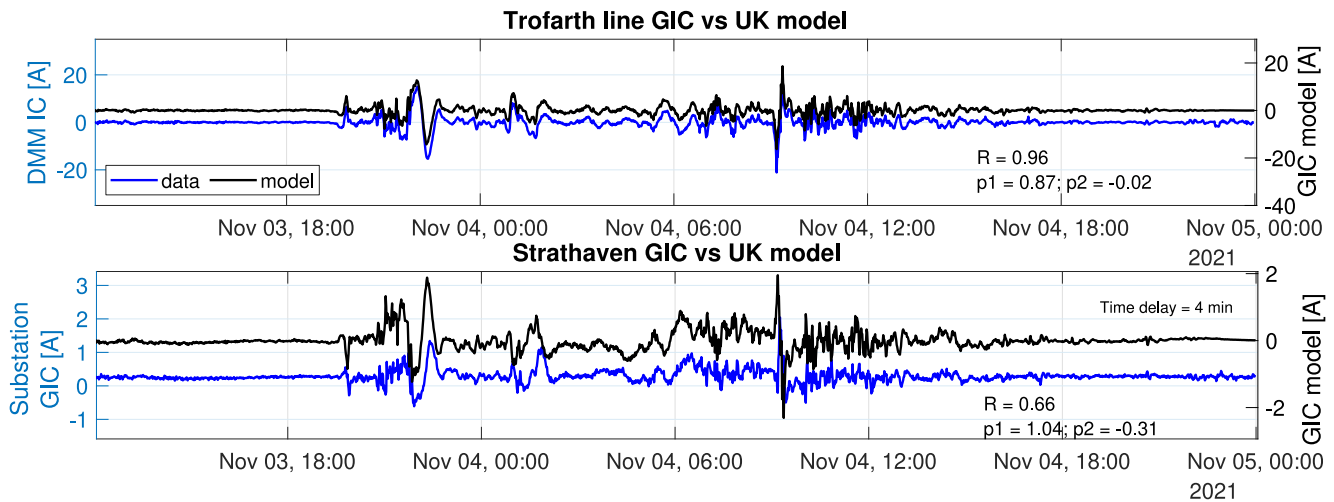


Figure 8. Top panel: Measured (left axis, blue) and modeled (right axis, black) line GICs derived from DMM data at Trofarth (TRO) in NW Wales. Lower panel: Measured (left axis, blue) and modeled (right axis, black) substation GIC for site Strathaven in Scotland 3–5 November 2021. For locations see Figure 1. Correlation coefficient and polynomial fit coefficients are also displayed. Substation GIC data were provided by Scottish Power Ltd.

suggest that a delayed GIC response is possible in parts of the HV grid for larger geomagnetic events. The amplitude of the modeled GIC values are recovered very closely at EAS ($p1 = 0.89$), but underestimated at KNA ($p1 = 0.56$), TOP ($p1 = 0.60$) and Strathaven ($p1 = 0.40$).

4.4. 11 May 2021 Storm: EAS, DAL

This event was classified as a G3 strong geomagnetic storm and reached a maximum K_{ESK} value of 7 and $a_p = 132$. Two of the DMM sites were recording (EAS and DAL in Scotland). The largest observed line GICs were 16 A at DAL and 26 A at EAS on 12 May 2021 12:21 GMT. Electric fields at both sites were calculated using the MT impedance derived from measurements at DAL. Correlation between modeled and measured signal is very high with values of 0.97, as shown in Figure 7. Both sites are relatively close to each other (40 km), and the availability of MT data at one site increases the confidence in a more accurate geoelectric field estimate. The amplitude of the recovered signal is very close to the measured one (DAL $p1 = 0.86$; EAS $p1 = 0.96$).

4.5. 3 November 2021 Storm: TRO, STHA

This was the most active geomagnetic period classified as a G4 severe storm with K_{ESK} reaching 8 and a planetary $a_p = 179$. Unfortunately only one of the DMM sites was still active (TRO in North Wales) given the challenging nature of field work that year. The maximum observed line GIC was 21 A on 4 November 2021 09:11 GMT (see Figure 8).

Scottish Power Ltd. provided ground GIC data measured at the substation Strathaven in Scotland with maximum values of about 2 A. Modeling the substation GIC at Strathaven using ESK magnetic field values and the DAL MT impedance produced a comparable estimate of transformer GIC with a correlation factor of 0.66 and a compatible amplitude ($p1 = 1.04$). We also observe a 4 min time delay between the maximum of observed and modeled GIC.

The geoelectric field in North-West Wales is very variable spatially. We compared the modeled electric field at three sites surrounding the DMM site TRO (see Figure 9). We find that peak amplitudes for E_y range from 36 mV at SH54 Southwest of TRO, 30 mV at SJ06 in the Southeast to 430 mV at SH39 in the Northwest in North Anglesey (see Figure 10, upper three rows). In order to account for this we used geometrically interpolated values from all three sites to derive the ground electric field values at TRO (see Figure 10, lowest row). Using this estimate allows a very accurate model of line GICs at Trofarth to be computed (Figure 8, upper panel, R value of 0.96 and $p1 = 0.87$). This demonstrates that the better we can make the local geoelectric field model using MT impedances, the closer the GIC model fits to the measured data.

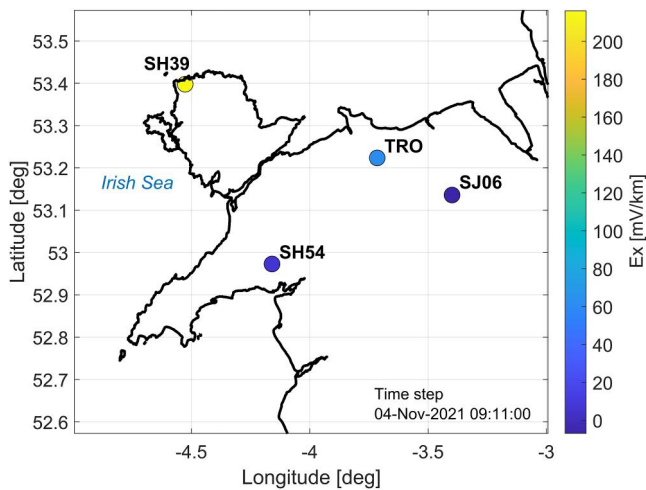


Figure 9. Location of MT and DMM sites in NW Wales. Circles on the map indicate electric field E_x (North–South) values for a time snapshot on 4 November 2021 09:11:00 (GMT + 1), during the period of increased geomagnetic activity.

5. Discussion

From the examples described in the previous section, we demonstrate that the GIC values output by the high-voltage network model are sufficiently close to the measurements made at the 10 DMM site to validate it (within the known uncertainties).

The signal shape of the modeled GICs strongly resemble the measured values. At most sites (ASB, KNA, WHI, TOP, EAS, DAL, and TRO) the amplitude of the GICs are correct within 20%. At a few sites (ILD, BRA and STHA) the amplitude is underestimated, whereas for TORN it is overestimated. These remaining uncertainties can be attributed to (a) the assumptions made in the HV model on the substation level and (b) the accuracy of the predicted geoelectric field which is still limited here to a point measurement due to the scarcity of MT measurements. At the time of writing, a field campaign to collect MT data all around Great Britain is underway and future estimates of the geoelectric field can be based on these new measurements.

There is some additional uncertainty about the actual configuration of the HV grid at the time of each recording. HV lines and substations are often switched on or off to meet demand and to accommodate other factors like maintenance schedules or damaged equipment. These are ultimately controlled by the grid operator on a very short time scale and it is currently not possible to input these dynamic changes into our model.

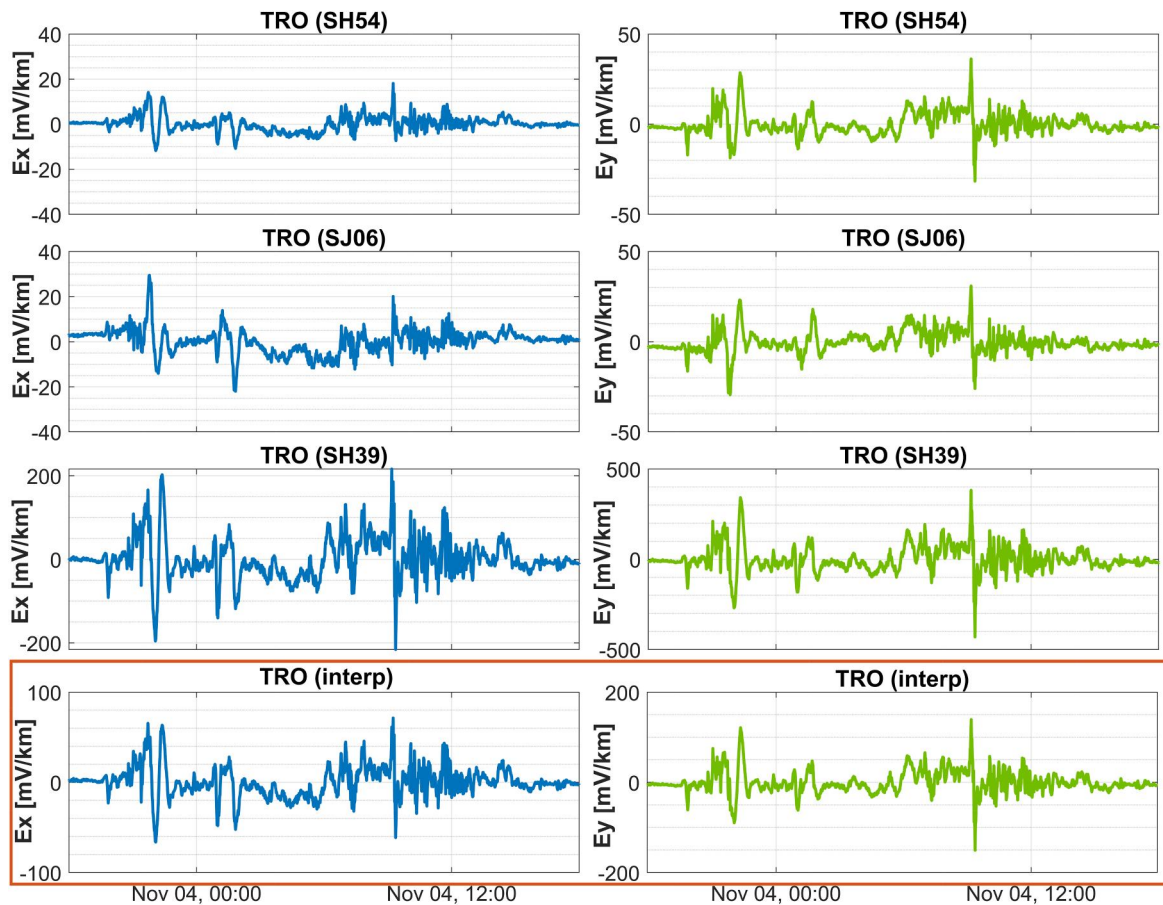


Figure 10. Modeled electric field at site TRO 3–5 November 2021 using MT impedance data from three surrounding sites. Blue lines—modeled E_x (N–S directed electric field), green lines—modeled E_y (E–W directed electric field). Orange box: interpolated electric fields from three MT locations.

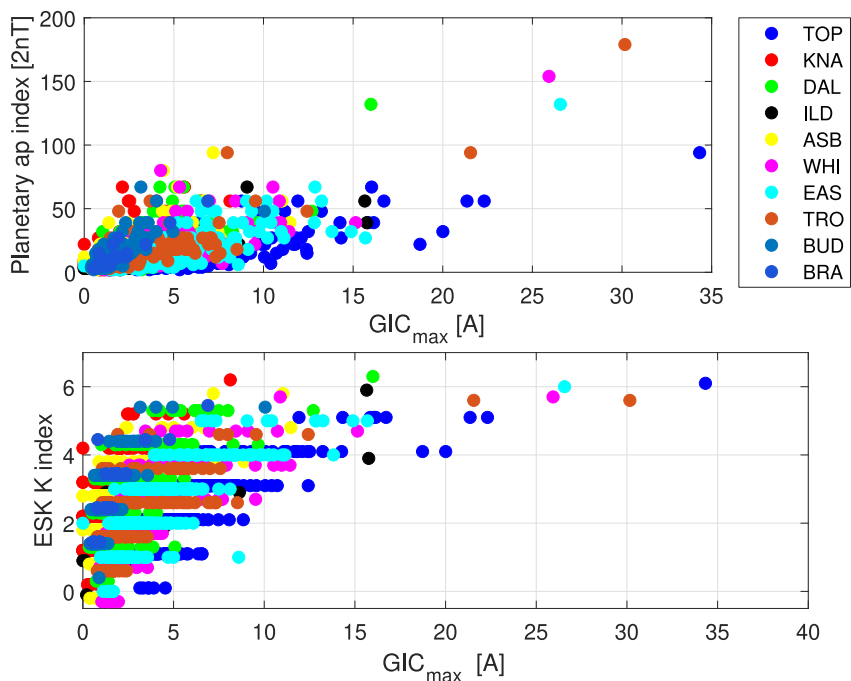


Figure 11. Planetary ap index (top panel) and K index at Eskdalemuir observatory (lower panel) against all daily GIC maximum estimates for each of the DMM sites 2018–2022. Each DMM site is color-coded. This highlights how varied the levels of line GIC flowing at different points in the grid are.

In general, the recorded line GICs vary strongly across the UK HV network. Figure 11 shows the relationship between geomagnetic activity and the GIC estimated at each site. As the measurement campaign took place during solar minimum there were few examples of large storms when many of the DMM sites were active. The largest GIC were observed at WHI, DAL, and EAS in Scotland, TOP in England and TRO in Wales during active periods.

We find that the modeled line GIC correlate much better with the measured GIC values when the appropriate MT impedance is used to generate the geoelectric field driving the line currents. In the case of the WHI data, the local impedance function is better than the Eskdalemuir values. However, at the closest substation, Torness, the geoelectric field produced by the Eskdalemuir impedance function produced a closer match overall than the WHI impedance function. This may be because the ESK MT impedance better represents the wider regional geoelectric field, but only more MT measurements in the area can reduce this uncertainty.

In a more geologically complex location in North Wales, MT impedances from three closely located sites were found to create a much more representative geoelectric field and an excellent match for TRO compared to any single MT site alone, which would either largely over or underestimate the amplitude of the geoelectric field. From this we conclude that correctly modeling the geoelectric field is very important and it is best to use MT measurements from several proximal sites where feasible.

For the modeling of GICs in substations, we unfortunately only have access to data from two substations in Scotland which limits the conclusions we can draw. From the comparisons of the available measured data, it is clear from the results presented in Figures 5, 6, and 10 that substation GICs do not correlate as highly as line GIC and the amplitude of the modeled signal is less accurate. There are several possible explanations for the disagreement. First, the HV model does not include specific earthing resistance measurements at each substation. Instead, all earthing resistances are fixed at 0.5Ω in the model. Second, we do not know which transformers are active within a substation during a given storm, which means the behavior of the GIC is not quite in accordance with the model. Finally, the information used to produce the model is from open source documents which do not necessarily reflect the true network.

6. Conclusions

In this study, we present DMM data collected in mainland Britain during 2018–2022. Although conducted during the quiet part of solar cycle 24, the campaign captured several geomagnetic storm times. We recorded line GIC data at 12 locations and present measured and modeled GICs for nine sites with sufficient data quality for five periods of increased geomagnetic activity. For modeling the ground electric field we used MT data collected at locations close to the DMM sites and find that this produces a good to very good fit between measured and modeled values. For a site in north Wales we used an interpolated estimate using three MT site to achieve the best fit between model and data. In addition we modeled GIC data measured at two substations in Scotland. At both sites the data are reasonably well fitted, although with less accuracy than for the line GICs.

The presented study shows that both the used HV network representation and GIC model work very well in combination with realistic ground electric field values derived from magnetic field observations and MT data to explain observed GICs. In the absence of comprehensive GIC monitoring in the UK power grid, the DMM data set provides multiple validation points both spatially across the grid as well as in time with several moderate geomagnetic events observed.

In the future, the country-wide geoelectric field model will be based on MT measurements currently being collected in the UK. Eliminating remaining uncertainties regarding grid parameters will further increase the accuracy of our GIC modeling capability.

Data Availability Statement

All DMM data, MT data and GIC data are openly available from the National Geoscience Data Centre (<https://www.bgs.ac.uk/services/ngdc/>). *K* index data for Eskdalemuir and planetary ap index can be obtained from the BGS website: https://geomag.bgs.ac.uk/data_service/data/home.html.

Acknowledgments

We thank the BGS Geomagnetism engineering team for their work in designing, building and testing the differential magnetometer equipment and providing fieldwork assistance. We thank the landowners who granted access for installing DMM equipment. This work was funded under UK Natural Environment Research Council Grant NE/P017231/1 “Space Weather Impact on Ground-based Systems (SWIGS).” MT data were collected during a country-wide field campaign in 2021–2023 under the SWIMMR (Space Weather Instrumentation Monitoring and Modelling) N4 project funded by the UK Natural Environment Research Council Grant NE/V002694/1. We thank two anonymous reviewers for comments that helped improve the manuscript. This paper is published with the permission of the Executive Director of the British Geological Survey (UKRI).

References

- Albert, D., Schachinger, P., Bailey, R. L., Renner, H., & Achleitner, G. (2022). Analysis of long-term GIC measurements in transformers in Austria. *Space Weather*, 20(1), e2021SW002912. <https://doi.org/10.1029/2021SW002912>
- Albertson, V. D., Kappenman, J. G., Mohan, N., & Skarbakka, G. A. (1981). Load-flow studies in the presence of geomagnetically-induced currents. *IEEE Transactions on Power Apparatus and Systems*, 100(2), 594–607. <https://doi.org/10.1109/TPAS.1981.316916>
- Alves Ribeiro, J., Pinheiro, F. J. G., & Pais, M. A. (2021). First estimations of geomagnetically induced currents in the south of Portugal. *Space Weather*, 19(1), e2020SW002546. <https://doi.org/10.1029/2020SW002546>
- Beamish, D., Clark, T. D. G., Clarke, E., & Thomson, A. W. P. (2002). Geomagnetically induced currents in the UK: Geomagnetic variations and surface electric fields. *Journal of Atmospheric and Terrestrial Physics*, 64(16), 1779–1792. [https://doi.org/10.1016/S1364-6826\(02\)00127-X](https://doi.org/10.1016/S1364-6826(02)00127-X)
- Beggan, C. (2015). Sensitivity of geomagnetically induced currents to varying auroral electrojet and conductivity models. *Earth Planets and Space*, 67(1), 1–12. <https://doi.org/10.1186/s40623-014-0168-9>
- Beggan, C., Beamish, D., Richards, A., Kelly, G. S., & Thomson, A. W. P. (2013). Prediction of extreme geomagnetically induced currents in the UK high-voltage network. *Space Weather*, 11(7), 407–419. <https://doi.org/10.1002/swe.20065>
- Blake, S. P., Gallagher, P. T., Campanya, J., Hogg, C., Beggan, C. D., Thomson, A. P., et al. (2018). A detailed model of the Irish high voltage power network for simulating GICs. *Space Weather*, 16(11), 1770–1783. <https://doi.org/10.1029/2018SW001926>
- Bolduc, L. (2002). GIC observations and studies in the Hydro-Québec power system. *Journal of Atmospheric and Solar-Terrestrial Physics*, 64(16), 1793–1802. [https://doi.org/10.1016/S1364-6826\(02\)00128-1](https://doi.org/10.1016/S1364-6826(02)00128-1)
- Boteler, D. H. (2006). The super storms of August/September 1859 and their effects on the telegraph system. *Advances in Space Research*, 38(2), 159–172. <https://doi.org/10.1016/j.asr.2006.01.013>
- Boteler, D. H. (2019). A 21st century view of the March 1989 magnetic storm. *Space Weather*, 17(10), 1–15. <https://doi.org/10.1029/2019SW002278>
- Butala, M. D., Kazerooni, M., Makela, J. J., Kamalabadi, F., Gannon, J. L., Zhu, H., & Overbye, T. J. (2017). Modeling geomagnetically induced currents from magnetometer measurements: Spatial scale assessed with reference measurements. *Space Weather*, 15(10), 1357–1372. <https://doi.org/10.1002/2017SW001602>
- Campanya, J., Gallagher, P. T., Blake, S. P., Gibbs, M., Jackson, D., Beggan, C. D., et al. (2019). Modeling geoelectric fields in Ireland and the UK for space weather applications. *Space Weather*, 17(2), 216–237. <https://doi.org/10.1029/2018SW001999>
- Campbell, W. H. (1980). Observation of electric currents in the Alaskan oil pipeline resulting from auroral electrojet current sources. *Geophysical Journal of the Royal Astronomical Society*, 61(2), 437–449. <https://doi.org/10.1111/j.1365-246X.1980.tb04325.x>
- Cliilverd, M. A., Rodger, C. J., Brundell, J. B., Dalzell, M., Martin, I., Mac Manus, D. H., et al. (2018). Long-lasting geomagnetically induced currents and harmonic distortion observed in New Zealand during the 7–8 September 2017 disturbed period. *Space Weather*, 16(6), 704–717. <https://doi.org/10.1029/2018SW001822>
- Divett, T., Mac Manus, D. H., Richardson, G. S., Beggan, C. D., Rodger, C. J., Ingham, M., et al. (2020). Geomagnetically induced current model validation from New Zealand’s South Island. *Space Weather*, 18(8), e2020SW002494. <https://doi.org/10.1029/2020SW002494>
- Hübner, J., Beggan, C. D., Richardson, G. S., Martyn, T., & Thomson, A. W. P. (2020). Differential magnetometer measurements of geomagnetically induced currents in a complex high voltage network. *Space Weather*, 18(4), e2019SW002421. <https://doi.org/10.1029/2019SW002421>

- Hughes, J., Mcgranaghan, R., Kellerman, A. C., Bortnik, J., Arritt, R. F., Venkataramani, K., et al. (2022). Revealing novel connections between space weather and the power grid: Network analysis of ground-based magnetometer and geomagnetically induced currents (GIC) measurements. *Space Weather*, *20*(2), e2021SW002727. <https://doi.org/10.1029/2021SW002727>
- Kelly, G. S., Viljanen, A., Beggan, C. D., & Thomson, A. W. P. (2017). Understanding GIC in the UK and French high-voltage transmission systems during severe magnetic storms. *Space Weather*, *15*(1), 99–114. <https://doi.org/10.1002/2016SW001469>
- Love, J. J., Lucas, G. M., Kelbert, A., & Bedrosian, P. A. (2018). Geoelectric hazard maps for the Mid-Atlantic United States: 100 year extreme values and the 1989 magnetic storm. *Geophysical Research Letters*, *45*(1), 5–14. <https://doi.org/10.1002/2017GL076042>
- Mac Manus, D. H., Rodger, C. J., Dalzell, M., Thomson, A. W. P., Clilverd, M. A., Petersen, T., et al. (2017). Long-term geomagnetically induced current observations in New Zealand: Earth return corrections and geomagnetic field driver. *Space Weather*, *15*(8), 1020–1038. <https://doi.org/10.1002/2017SW001635>
- Marsal, S., Torta, J. M., Curto, J. J., Canillas-Perez, V., Cid, O., Ibanez, M., & Marcuello, A. (2021). Validating GIC modeling in the Spanish power grid by differential magnetometry. *Space Weather*, *19*(12), e2021SW002905. <https://doi.org/10.1029/2021SW002905>
- Marshall, R. A., Dalzell, M., Waters, C. L., Goldthorpe, P., & Smith, E. A. (2012). Geomagnetically induced currents in the New Zealand power network. *Space Weather*, *10*(8), S08003. <https://doi.org/10.1029/2012SW000806>
- Matandirotya, E., Cilliers, P. J., Van Zyl, R. R., Oyedokun, D. T., & de Villiers, J. (2016). Differential magnetometer method applied to measurement of geomagnetically induced currents in Southern African power networks. *Space Weather*, *14*(3), 221–232. <https://doi.org/10.1002/2015SW001289>
- McKay, A. (2003). Geoelectric fields and geomagnetically induced currents in the United Kingdom. Doctoral dissertation. University of Edinburgh. Retrieved from <https://era.ed.ac.uk/handle/1842/639>
- Myllys, M., Viljanen, A., Rui, O. A., & Ohnstad, T. M. (2014). Geomagnetically induced currents in Norway: The northernmost high-voltage power grid in the world. *Journal of Space Weather and Space Climate*, *4*, A10. <https://doi.org/10.1051/swsc/2014007>
- NOAA National Centers for Environmental Information. (2022). ETOPO 2022 15 arc-second global relief model. <https://doi.org/10.25921/fd45-gt74>
- Oughton, E. J., Hapgood, M., Richardson, G. S., Beggan, C. D., Thomson, A. W. P., Gibbs, M., et al. (2018). A risk assessment framework for the socioeconomic impacts of electricity transmission infrastructure failure due to space weather: An application to the United Kingdom. *Risk Analysis*, *38*(12), 1–22. <https://doi.org/10.1111/risa.13229>
- Oughton, E. J., Skelton, A., Horne, R. B., Thomson, A. W. P., & Gaunt, C. T. (2017). Quantifying the daily economic impact of extreme space weather due to failure in electricity transmission infrastructure. *Space Weather*, *15*(1), 65–83. <https://doi.org/10.1002/2016SW001491>
- Pulkkinen, A., Bernabeu, E., Eichner, J., Beggan, C., & Thomson, A. (2012). Generation of 100-year geomagnetically induced current scenarios. *Space Weather*, *10*(4), S04003. <https://doi.org/10.1029/2011SW000750>
- Pulkkinen, A., Bernabeu, E., Thomson, A., Viljanen, A., Pirjola, R., Boteler, D., et al. (2017). Geomagnetically induced currents: Science, engineering, and applications readiness. *Space Weather*, *15*(7), 828–856. <https://doi.org/10.1002/2016SW001501>
- Pulkkinen, A., Viljanen, A., Pajunpaa, K., & Pirjola, R. (2001). Recordings and occurrence of geomagnetically induced currents in the Finnish natural gas pipeline network. *Journal of Applied Geophysics*, *48*(4), 219–231. [https://doi.org/10.1016/S0926-9851\(01\)00108-2](https://doi.org/10.1016/S0926-9851(01)00108-2)
- Rodger, C. J., Mac Manus, D. H., Dalzell, M., Thomson, A. W., Clarke, E., Petersen, T., et al. (2017). Long-term geomagnetically induced current observations from New Zealand: Peak current estimates for extreme geomagnetic storms. *Space Weather*, *15*(11), 1447–1460. <https://doi.org/10.1002/2017SW001691>
- Rosenqvist, L., Fristedt, T., Dimmock, A. P., Davidsson, P., Fridström, R., Hall, J. O., et al. (2022). 3D modeling of geomagnetically induced currents in Sweden—Validation and extreme event analysis. *Space Weather*, *20*(3), e2021SW002988. <https://doi.org/10.1029/2021SW002988>
- Rosenqvist, L., & Hall, J. O. (2019). Regional 3-D modeling and verification of geomagnetically induced currents in Sweden. *Space Weather*, *17*(1), 27–36. <https://doi.org/10.1029/2018SW002084>
- Saadat, H. (2010). *Power system analysis* (3rd ed.). PSA Publishing LLC.
- Schofield, D. I., Leslie, A. G., Wilby, P. R., Dartnall, R., Waldron, J. W. F., & Kendall, R. S. (2021). Tectonic evolution of Anglesey and adjacent mainland North Wales. *Geological Society, London, Special Publications*, *503*(1), 371–390. <https://doi.org/10.1144/SP503-2020-9>
- Thomson, A. W. P., McKay, A. J., Clarke, E., & Reay, S. J. (2005). Surface electric fields and geomagnetically induced currents in the Scottish Power grid during the 30 October 2003 geomagnetic storm. *Space Weather*, *3*(11), S11002. <https://doi.org/10.1029/2005SW000156>
- Turnbull, K. (2010). Modelling GIC in the UK. *Astronomy and Geophysics*, *51*(5), 25–26. <https://doi.org/10.1111/j.1468-4004.2010.51525.x>
- Viljanen, A., & Pirjola, R. (1994). Geomagnetically induced currents in the Finnish high-voltage power system. *Surveys in Geophysics*, *15*(4), 383–408. <https://doi.org/10.1007/BF00665999>
- Yang, B., Egbert, G. D., Zhang, H., Meqbel, N., & Hu, X. (2021). Electrical resistivity imaging of continental United States from three-dimensional inversion of EarthScope USArray magnetotelluric data. *Earth and Planetary Science Letters*, *576*, 117244. <https://doi.org/10.1016/j.epsl.2021.117244>